A deeper insight into the dual temperature- and pH-responsiveness of poly(vinylamine)-b-poly(N-isopropylacrylamide) double hydrophilic block copolymers

Clémence Nadal, Stéphane Gineste, Olivier Coutelier, Audrey Tourrette, Jean-Daniel Marty, Mathias Destarac

Version of Record: https://www.sciencedirect.com/science/article/pii/S0927775722002564
Manuscript_426b9cce2867adc1290b89fa7eff28e3

A deeper insight into the dual temperature- and pH-responsiveness of poly(vinylamine)-*b*-poly(N-isopropylacrylamide) double hydrophilic block copolymers

Clémence Nadal[1,2], Stéphane Gineste[2], Olivier Coutelier[2], Audrey Tourrette[1], Jean-Daniel Marty[2*], Mathias Destarac[2*]

[1] CIRIMAT, CNRS UMR 5085, Université de Toulouse, Université Toulouse III - Paul Sabatier, 31062 Toulouse, France.

[2] IMRCP, CNRS UMR 5623, Université de Toulouse, Université Toulouse III - Paul Sabatier, 31062 Toulouse, France.

* corresponding authors: mathias.destarac@univ-tlse3.fr and jean-daniel.marty@univ-tlse3.fr

Highlights

- A thorough study of the critical transition of PVAm-*b*-PNIPAM copolymers as a function of pH and molar mass revealed that the mean cloud point temperature is around 38 °C
- An aggregation study revealed that such copolymers when fully protonated undergo a transition from a randomly aggregated state to a structured core-shell form
- Core-shell nanoparticles were observed at pH 5 and 45 °C by light and X-ray scattering and are most likely composed of a dense PNIPAM core of 20 nm diameter and a hydrated PVAm shell of 15 nm thickness.

Abstract

Block copolymers based on poly(vinylamine) and poly(*N*-isopropylacrylamide), $PVAm_m$-*b*-$PNIPAM_n$, were synthetized by hydrazinolysis of poly(*N*-vinylphthalimide) based copolymers, $PVPI_m$-*b*-$PNIPAM_n$, obtained by RAFT polymerization. The effect of molar mass and pH on the thermoresponsive and aggregation properties of these polymers in aqueous solution was studied with UV-vis spectroscopy, differential scanning calorimetry, NMR spectrometry, light and X-ray scattering experiments. For the first time it was demonstrated that at room temperature, these copolymers are prone to self-assemble and tend to form larger aggregates upon heating. Hence core-shell nanostructures with a dense PNIPAM core and a hydrophilic PVAm shell, were notably observed above T_c when pH < pKa.

Graphical abstract

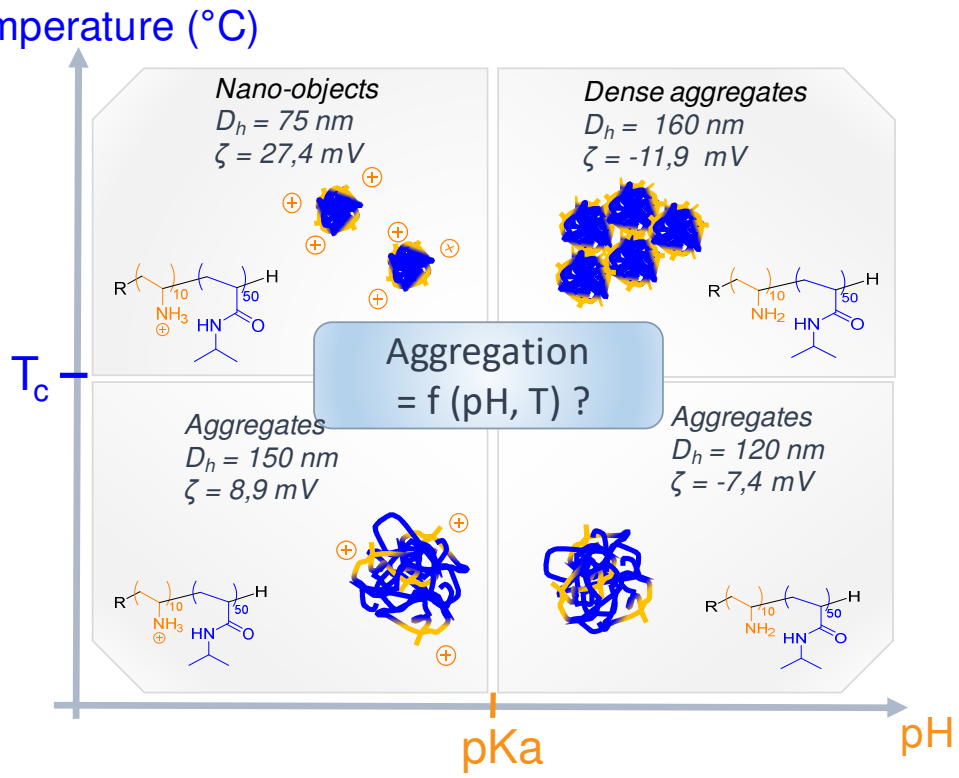

Keywords

block copolymers / self-assembly / thermoresponsive/ pH-sensitive

1. Introduction

Due to their wide range of application, amphiphilic copolymers represent more than ever a vast area of research. When dispersed in aqueous media, amphiphilic block copolymers display opposite behaviour, resulting in the reorganization of the two blocks to fit their affinities and self-assemble [1,2, 3]. Alternatively, stimuli-responsive polymers need a trigger to assemble in solution in response to different stimuli such as temperature, electrical or magnetic field and mechanical stress, pH, ionic strength or addition of a chemical [4,5].

Among them, thermoresponsive polymers which display Lower- or Upper Critical Solution Temperature (LCST or UCST), are of special interest because of their high potential in drug delivery and tissue engineering [6,7]. Most reported LCST polymers are poly(vinylcaprolactam) (PVCL) [8], ethylene glycol-based copolymers including poly(oligo(ethylene glycol) methyl ether (meth)acrylates) [9-12], and polyacrylamides, e.g poly(*N*-isopropylacrylamide) (PNIPAM) [13-14]. The presence of pendant amide groups and their ability to form hydrogen bonds, as well as the hydrophobic/hydrophilic balance between the carbon backbone and the polar amide groups is responsible for the LCST behavior of acrylamides in solution [15]. The LCST-type phase transition of PNIPAM is induced by a coil-to-globule transition induced by dehydration of polymer chains at a temperature around 32°C [16]. The incorporation of hydrophilic or hydrophobic comonomers in PNIPAM allows fine-tuning of the cloud point temperature (T_c) [17-18]. For example, when NIPAM monomer is statistically copolymerized with hydrophilic monomers such as acrylamide, T_c increases up to about 45 °C when the polymer chain comprises 18 mol % of acrylamide, whereas T_c decreases to about 23 °C when 20 mol % of hydrophobic N-tert-butylacrylamide is incorporated into the polymer chain [19]. Although this effect is less pronounced than for statistical copolymers, it can still be observed in block copolymers. Double-hydrophilic LCST block copolymers for instance usually have an upper-shifted LCST [20].

Stimuli-responsive double-hydrophilic block copolymers are attractive materials since they can be fully miscible in water until a stimulus such as temperature or pH is applied, inducing their self-assembly. Hence, PNIPAM-based thermoresponsive DHBCs were extensively studied for their ability to form thermally responsive micelles, where PNIPAM forms the core above LCST. [21] PNIPAM-b-PEG copolymers were indeed used as lipophilic drug nanocarriers for which a decrease of temperature below the LCST induces the disassembly of core-shell structure and consequently a drug release. [22-24] Attaching a positively or negatively charged block to a neutral polymer is another way to tune its self-assembly by using pH and/or ionic strength as stimuli [25]. Commonly used pH-sensitive polymers are poly(acrylic acid) (PAA), poly(methacrylic acid) (PMAA) and poly(2-(dimethylamino)ethyl methacrylate) (PDMAEMA) [26]. Poly(vinylamine) (PVAm) displays a good

solubility in water over a large range of pH (2-11) and a polyelectrolyte behavior, which aroused the interest of multiple research teams [27]. Mori *et al.* have reported for the first time the synthesis of PVAm with controlled macromolecular characteristics from the polymerization of N-vinylphthalimide (NVPI) by reversible addition-fragmentation chain transfer (RAFT) polymerization followed by the deprotection of phthalimido groups with hydrazine. By using this method, the synthesis of PVAm homopolymer [28], alternating copolymers with other monomers such as NIPAM [29], and finally PVAm-*b*-PNIPAM and zwitterionic (PVAm-*b*-PALysOH) block copolymers were reported as well as their physicochemical behavior in aqueous solution [30-31]. The self-assembly and stability properties of polyplex micelles obtained from the complexation of anionic DNA with these block copolymers was more specifically studied [31].

As depicted in **Figure 1**, depending on pH and temperature each block in PVAm-*b*-PNIPAM copolymer should present different protonation states or conformations in solution. Also, intra- and inter-block hydrogen bonding interactions between amine, ammonium and amide groups are expected. At pH below pKa, the PVAm block is in the highly hydrophilic ammonium form, whereas at pH well above pKa, the amine form is predominant. Concerning the PNIPAM block, it is in a hydrated form below its critical temperature and upon heating undergoes a coil-to-globule transition due to partial dehydration of PNIPAM chains. These structural modifications will condition the solution properties of the polymers. The objective of this study is therefore to focus on the aggregation behavior of PVAm-*b*-PNIPAM block copolymers as a function of pH and temperature in order to bring out a deeper understanding of their complex self-assembly behaviour [31].

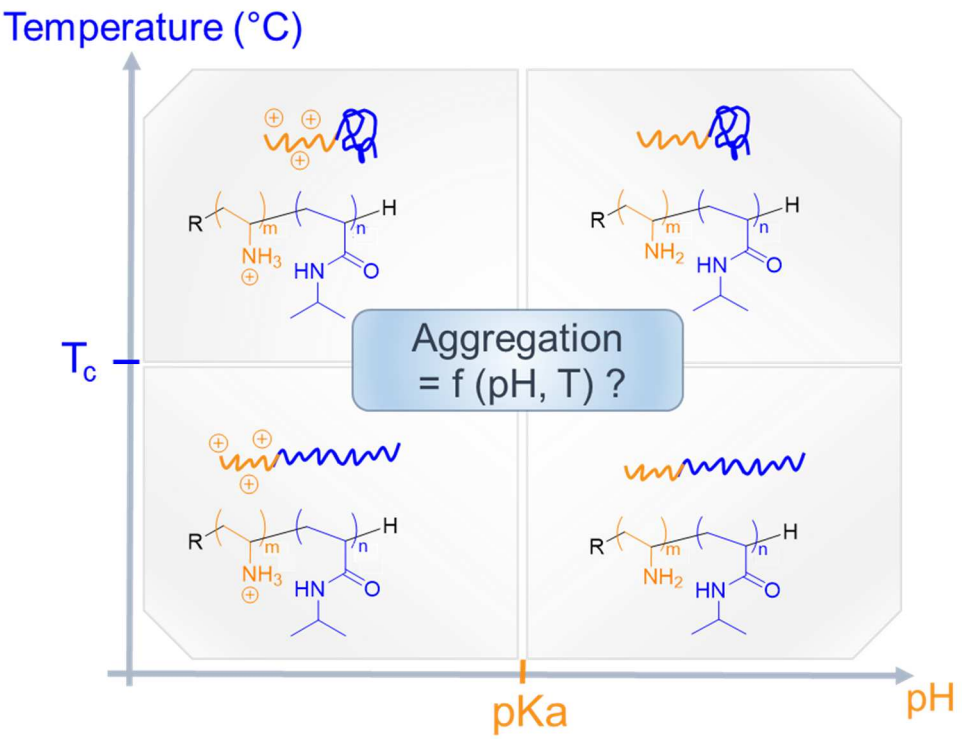

***Figure 1**. PVAm$_m$-b-PNIPAM$_n$ structure and schematic representation as a function of cloud point temperature and pKa*

First, the synthesis of PVAm$_{10}$-*b*-PNIPAM$_{50}$ and PVAm$_{20}$-*b*-PNIPAM$_{100}$ copolymers was escribed. Then, the phase transition temperature of both copolymers was studied through the determination of cloud point temperature T_c by scattering, NMR, spectroscopy and microscopy methods, at pH < pKa and pH > pKa. We found interesting to assess the influence of the protonation degree of the PVAm block on the T_c values of the block copolymers. Finally, dynamic light scattering (DLS) and small-angle X-Ray scattering (SAXS) experiments were carried out along with TEM imaging to investigate the aggregation properties of the copolymers in solution and to decipher for the first time the structure of such aggregates. Our final goal was the establishment of a morphological state phase diagram based on multi-angle DLS and SAXS experiments.

2. Experimental section

2.1. Materials

N-Vinylphthalimide (NVPI, 99%, Acros Organics), N-isopropylacrylamide (NIPAM, 97%, Aldrich), hydrazine monohydrate (98%, Sigma Aldrich), dilauroyl peroxide (LPO, 99%, Acros Organics), methanol (99.9%, Sigma-Aldrich), N-N-dimethylformamide (DMF, 99.9%, Sigma-Aldrich), diethyl ether (99.9% Sigma-Aldrich), 1,4-dioxane (VWR) were used as received. 2,2-Azobisisobutyronitrile (AIBN, 98%, Acros Organics) was purified by recrystallization with methanol. *O*-ethyl-*S*-(1-methoxycarbonyl) ethyldithiocarbonate (Xanthate XA1) was synthetized following a previously reported method [32]. Ultrapure water was obtained from a Elga Purelab Flex device with resistivity value under 18 MΩ/cm. Dialysis were carried in 1 kDa cut-off dialysis tubes from GE Healthcare Bio-Sciences Corp.

2.2. PVAm$_n$-*b*-PNIPAM$_m$ synthesis

Synthesis of PVPI$_{10}$-b-PNIPAM$_{50}$-X. The synthesis of the PVPI$_{10}$-X macro-chain transfer agent (macro-CTA) was adapted from Maki *et al.* [28]. A typical RAFT polymerization procedure of NVPI is the following: NVPI (1.39 g, 8.0 mmol), Xanthate XA1 (154 mg, 0.74 mmol), AIBN (19 mg, 0.12 mmol) and DMF (4 mL) were introduced in a Schlenk tube. The mixture was degassed by four freeze-pump-thaw cycles and backfilled with argon before heating at 60 °C for 24 h. Conversion was determined by ^{1}H-NMR in DMSO-d6 of a crude sample. Finally, the obtained polymer was precipitated in diethyl ether, filtered off and dried under vacuum. Size-exclusion chromatography (SEC) and ^{1}H-NMR analyses were carried out to determine respectively $M_{n,\mathrm{MALS}}$ and $M_{n,\mathrm{NMR}}$ values.

A typical RAFT synthesis of PVPI$_{10}$-*b*-PNIPAM$_{50}$-X is as follows: in a Schlenk tube were introduced

NIPAM (2 g, 17.7 mmol), the previously synthesized $PVPI_{10}$-X (686 mg, 0.35 mmol), AIBN (12 mg, 0.07 mmol) and DMF (4 mL). The mixture was degassed by four freeze-pump-thaw cycles and backfilled with argon before heating at 65 °C for 16 h. A sample was collected for analysis by ^{1}H-NMR in DMSO-d6 to determine monomer conversion. Finally, the obtained polymer was precipitated in diethyl ether, filtered off and dried under vacuum. SEC analysis and ^{1}H-NMR analyses were carried out to determine respectively $M_{n,\mathrm{MALS}}$ and $M_{n,\mathrm{NMR}}$ values. The initial [Monomer]/[CTA] ratio was adapted to obtain the $PVPI_{20}$-*b*-$PNIPAM_{100}$-X with the initiator concentration kept constant with respect to the monomer concentrations.

Radical reduction of xanthate terminal group. The removal of the terminal xanthate group to obtain $PVPI_n$-*b*-$PNIPAM_m$ was carried out according to a previously reported procedure which is provided in ESI [33].

Hydrazinolysis of P VPI_{10}-b-$PNIPAM_{50}$. The hydrazinolysis procedure was adapted from Mori *et al*. [28] and carried out as follows: in a round-bottom flask was dissolved the $PVPI_{10}$-*b*-$PNIPAM_{50}$ copolymer (1.05 g, 0.646 mmol phthalimide units) in 12mL of a methanol/dioxane mixture with a 2/1 volume ratio. Hydrazine monohydrate (646 mg, 12.9 mmol) was introduced and the mixture degassed by bubbling argon for 1 h. The flask was equipped with a reflux condenser and the mixture was kept under reflux (85 °C) for 6 h. The heating was then stopped and solvents were removed under vacuum. The resulting oil was dissolved in MeOH/aqueous HCl (0.5M) with a 2/1 volume ratio. The $PVAm_n$-*b*-$PNIPAM_m$ copolymer was finally precipitated in diethyl ether, filtered off, dried under vacuum and dialyzed at pH > 9 against ultrapure water for 4 days. The final copolymer was recovered by lyophilization and used as such for physicochemical characterizations.

2.3. Methods.

Nuclear Magnetic Resonance (NMR). ^{1}H-NMR spectra were recorded at 300 MHz on a Bruker Advance 300 MHz spectrometer. ^{1}H-NMR in temperature was carried on a Bruker Advance 400 MHz spectrometer. DMSO-d6 was used for all PVPI-containing samples, D_2O was used for PVAm-based copolymers.

pH-titration. The pKa of the PVAm10-b-PNIPAM50 copolymer was determined by pH-titration of a polymer solution at a concentration equal to 3 mg/mL solubilized in 0.15 mol·L-1 KCl(aq). Prior to titration, 20 µL of a 0.1 mol·L-1 HCl(aq) solution was added to ensure complete protonation of amine functions. The initial pH of titrated solution was equal to 4). Titration was then performed with a 0.1 mol·L-1 KOH(aq) solution.

Size Exclusion Chromatography (SEC). Samples were prepared in DMF-LiBr (10 mM) at 5 mg mL^{-1} and filtered on a PTFE 0.45 µm filter. SEC injections were performed with a 1.0 mL.min^{-1} flow rate on a

Dionex UltiMate 3000 UHPLC pump from Thermo Scientific equipped with two Tosoh columns (α-2500, 8.0 x 300 mm and α-3000, 8.0 x 300 mm). Columns were thermostatted at 55 °C in an oven. Multidetection was provided from a refractive index detector (RI) Wyatt Optilab rEX, a UV detector Varian ProStar 325 UV and a multi-angle light scattering (MALS) detector Wyatt MiniDawn TREOS. Absolute molar masses and dispersities were determined using RI and MALS detection. All data were processed with Astra7 software from Wyatt Technology.

Dynamic Light Scattering (DLS). Multi-angle DLS experiments were performed on a 3D LS spectrometer from LS instruments (Switzerland). Working with a laser at 660 nm, this instrument recorded the light scattered at angles between 15 and 150° (typically more than ca 60 values). Typical acquisition time for each angle was set to 30 s. Five correlograms were recorded for each angle. All DLS data were then analyzed using a laboratory made software program (named M-STORMS). Cumulant or NNLS (Non-Negative Least Squares) methods led to an estimation of the decay rate Γ for each angle. The linear dependency of Γ versus the square of the scattering vector q (Γ=q^2.D) gives the diffusion coefficient of the nano-objects and therefore their radius through the Stokes-Einstein equation: $D = (kT)/(6\pi\eta R_h)$ where T is the temperature and η the viscosity of the solution. The size error was estimated by the standard deviation of all the calculations (with cumulant and NNLS methods, ca 10-12 values per experiment) for all similar experiments (4 experiments). Multi-angle DLS experiments were performed in dilute condition (0,01%w/v) to prevent sedimentation and multi-scattering phenomena to occur.

Mono-angle DLS measurements were conducted using a Zetasizer Nano-ZS (Malvern Instruments, Ltd, UK) with integrated 4 mW He-Ne laser at λ = 633 nm. The light scattering intensity (at 173°) was measured with instrumental parameters set to constant values for all the samples. The correlation function (measured twice for each sample) was analyzed via the cumulant method to get the Z-average size of the colloids. The standard deviation in the intensity and Z-average size are found for each sample respectively around 2% and 1%. Samples were prepared at 1 $\%_{w/v}$ in ultrapure water.

UV-vis spectroscopy. Transmittance of polymer aqueous solutions was recorded at 500 nm and different temperature with a Cary 100 Bio spectrophotometer at different heating/cooling rates (0.5, 1, 2.5 and 5 $°C \cdot min^{-1}$). Cloud point temperatures were calculated from the determination of inflexion point of each transmittance curve, extrapolated to 0 $°C \cdot min^{-1}$.

Differential Scanning Calorimetry (DSC). The thermal properties of the polymers (in solution and in bulk) were determined by DSC using a Mettler Toledo DSC 1 STARe System Thermal Analysis calorimeter equipped with a Gas Controller GC200. Solution samples were sealed in impermeable crucibles of 120 µL. Transition temperatures were taken at the top of the peak on the thermogram

on heating and extrapolated the values obtained at different heating rates to 0 °C/min. The variation of enthalpy was measured as the temperature increased at a rate of 1 °C/min.

Small-Angle X-ray Scattering (SAXS). SAXS experiments were performed on a XEUSS 2.0 bench equipped with an internal copper source. X-ray beam energy was 8 keV. Samples were prepared at 10 $\%_{w/v}$ at pH 5 and 11. Measurements were acquired during a heating ramp between 20 and 50 °C. Data were processed using the software SasView. q is the scattering wave vector defined as $q = (4\pi/\lambda) \sin \vartheta/2$, λ being the wavelength ($\lambda \sim 1$ Å) and ϑ the scattering angle.

Transmission Electron Microscopy (TEM). TEM images were acquired on a Hitachi HT7700 device. Samples were prepared in thermostatted conditions (25 °C and 45 °C) by depositing a drop of the previously thermostatted polymer solution (0.5 mg/mL) on copper carbon grids (FCF400-CU from Electron Microscopy Sciences). Samples were let to dry then a drop of contrasting agent solution (uranyl acetate) was deposed as well.

3. Results and discussion

3.1. Synthesis of $PVAm_n$-*b*-$PNIPAM_m$ diblock copolymer

Poly(vinyl amine)-*b*-poly(N-isopropylacrylamide) copolymers $PVAm_m$-*b*-$PNIPAM_n$ with controlled molar mass and well-defined structures were synthesized as follows: a two-step RAFT polymerization strategy (**Figure 2**) based on the work of Mori and coworkers [28,30] was used starting from the RAFT polymerization of N-vinyl phthalimide (NVPI) with xanthate XA1 control agent, to form a first PVPI block terminated with a xanthate functionality $PVPI_m$-X. The polymerization of NIPAM in the presence of a $PVPI_n$-X macro-RAFT agent led to the formation of $PVPI_m$-*b*-$PNIPAM_n$-X diblock copolymer.

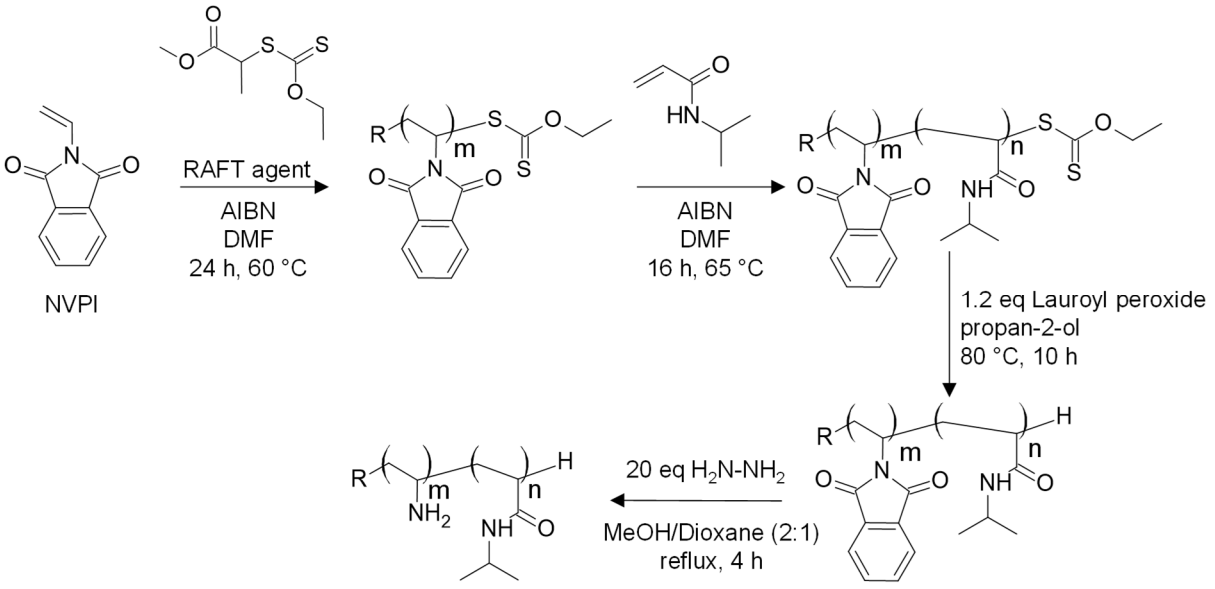

***Figure 2**. Synthesis pathway of $PVAm_{10}$-b-$PNIPAM_{50}$ via a 2-step RAFT polymerization to obtain $PVPI_{10}$-b-$PNIPAM_{50}$-X, followed by post-polymerization treatment*

$PVPI_{10}$-X and $PVPI_{20}$-X were obtained with NVPI conversion above 80 %. From these macro-CTAs, homothetic $PVPI_{10}$-*b*-$PNIPAM_{50}$-X and $PVPI_{20}$-*b*-$PNIPAM_{100}$-X copolymers were synthesized. NIPAM conversion was above 97 % for both copolymerizations. Chain extensions were confirmed by SEC analysis (**Figure S1**). M_n values of respectively 6900 g mol^{-1} and 15400 g mol^{-1} were obtained from SEC-MALS analysis. The terminal xanthate group was then removed by radical reaction with dilauroyl peroxide in propan-2-ol leading to $PVPI_m$-*b*-$PNIPAM_n$ copolymers. Finally, $PVPI_m$-*b*-$PNIPAM_n$ was reacted with an excess of hydrazine and converted into $PVAm_m$-*b*-$PNIPAM_n$. ^{1}H-NMR confirmed the deprotection of phthalimido groups with the disappearance of aromatic protons around 8 ppm (see **Figure S2**). $PVAm_m$-*b*-$PNIPAM_n$ copolymers were purified by dialysis to remove unreacted macro-CTA

from the diblock. A summary of the characteristics of PVAM$_m$-*b*-PNIPAM$_n$ is reported in **Table 1** below.

Table 1 Main characteristics of PVAM$_m$-b-PNIPAM$_n$ copolymers

	PVAm$_m$-*b*-PNIPAM$_n$ composition		
	DP_{VAm}/DP_{NIPAM} *th*	DP_{VAm}/DP_{NIPAM} *NMR* [(a)]	$M_{n,NMR}$ (g mol^{-1})
PVAm$_{10}$-*b*-PNIPAM$_{50}$	10/50	11/64	7700
PVAm$_{20}$-*b*-PNIPAM$_{100}$	20/100	17/110	13200

3.2. Thermoresponsive properties of PVAm$_m$-*b*-PNIPAM$_n$ copolymers

The behaviour in solution of PVAm-PNIPAM copolymers was studied as a function of pH and temperature. The amine functions of PVAm undergo a transition from protonated to non-protonated form for pH values above pKa, which is estimated in the case of PVAm homopolymer around 8.5 [27,34]. The pKa value of PVPI$_m$-*b*-PNIPAM$_n$ block copolymers determined from pH-metric titration (**Figure 3**) was found at a lower value of 7.54. This might be ascribed to the low degree of polymerization of the PVAm block in the studied copolymers. In addition, the protonation degree calculated according to Henderson-Hasselbalch equation is represented in **Figure 3**.

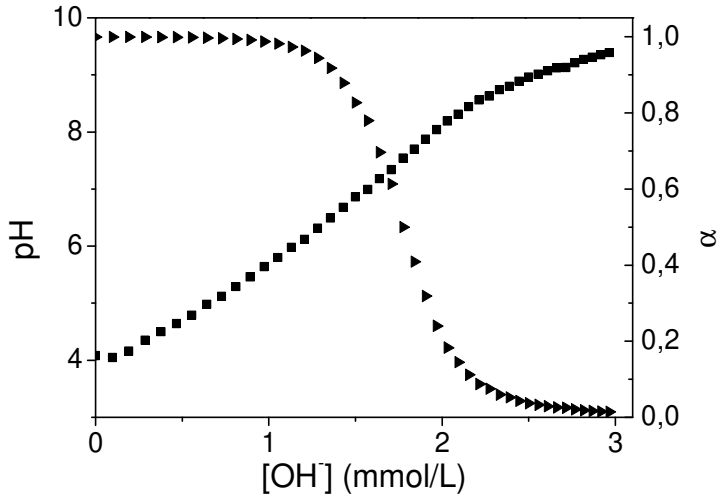

***Figure 3**. ■ Evolution of the pH and ▯ corresponding protonation degree (according to Henderson-Hasselbalch equation) of a PVAm$_{10}$-b-PNIPAM$_{50}$ polymer solution (3mg/mL) titrated with a KOH solution (0.1 mol.L^{-1}).*

In the following, the block copolymer solutions were prepared at three different pH values: one highly above pKa (pH 11) when the PVAm block is fully deprotonated (α ~ 0), the second around pKa (pH 8) with an intermediate protonation state (α between 0.2 et 0.8) and the last one well under (pH 5) so that PVAm is mostly protonated (α ~ 1). Each solution was characterized over a range of temperature between 25 °C and 55 °C. The homothetic $PVAm_{10}$-*b*-$PNIPAM_{50}$ and $PVAm_{20}$-*b*-$PNIPAM_{100}$ copolymers were studied. The solutions were noted as $PVAm_n$-*b*-$PNIPAM_m$@*pHx* with respectively n, m the number-average degree of polymerization of the blocks and x the pH of the solution. For each method, samples were prepared in ultrapure water (or D_2O when mentioned) at different concentrations and targeted pH of 5, 8 and 11. pH adjustment was made with diluted HCl and NaOH solutions (0.1 mol·L^{-1}). The effective pH of each sample is indicated in Table S1 of ESI.

Thermoresponsiveness at a pH value higher than pKa (pH 11).

The behaviour of $PVAm_{10}$-*b*-$PNIPAM_{50}$ polymer solutions was studied as a function of temperature thanks to UV-vis, DSC, light scattering and ^{1}H NMR techniques for concentrations ranging from 0.1 to 5 wt.%. Whatever the technique used, a sharp and reversible phase transition was observed. It should be noted that for most polymers, there is no significant difference in T_c values measured at different concentrations. Only PNIPAM homopolymers shows a significantly different value at 0.1 wt.% compared to the values assessed at 5 wt.%. **Figure 4a** presents the transmittance curves measured at 500 nm at different heating and cooling rates. A hysteresis phenomenon whose amplitude depends on the chosen heating/cooling rate is observed. This phenomenon is related to the difficulty of swelling compact aggregates formed at higher temperatures due to intra-chain entanglement.[34] Extrapolation of the estimated inflection on heating at null speed [35] enables the determination of the cloud point temperature T_c at 39.8°C (**Figure S3** in ESI). This value is, as expected, slightly higher than the value of PNIPAM homopolymer (i.e. 32 °C) due to the presence of the PVAm hydrophilic block. [36] T_c values equal to 36.4 and 36.0 °C were obtained on heating thanks to DSC and DLS experiments respectively at (**Figure S4-S5**). It should be noted that for these low molecular weight polymers, the study of thermal properties by UV-Vis spectroscopy leads to a systematic overestimation of T_c values compared to those obtained from DSC or DLS measurements. Such effects can be attributed to the need for these techniques to obtain aggregates of sufficient size to be detectable. Thus, even as the dehydration of the polymer chain begins, as evidenced by DSC measurements, the formation of aggregates of sufficient size able to scatter light at a sufficient level requires a certain amount of time and/or a greater dehydration level. Cloud points determined by these different characterization methods are given in **Table S2** and in **Table 2.**

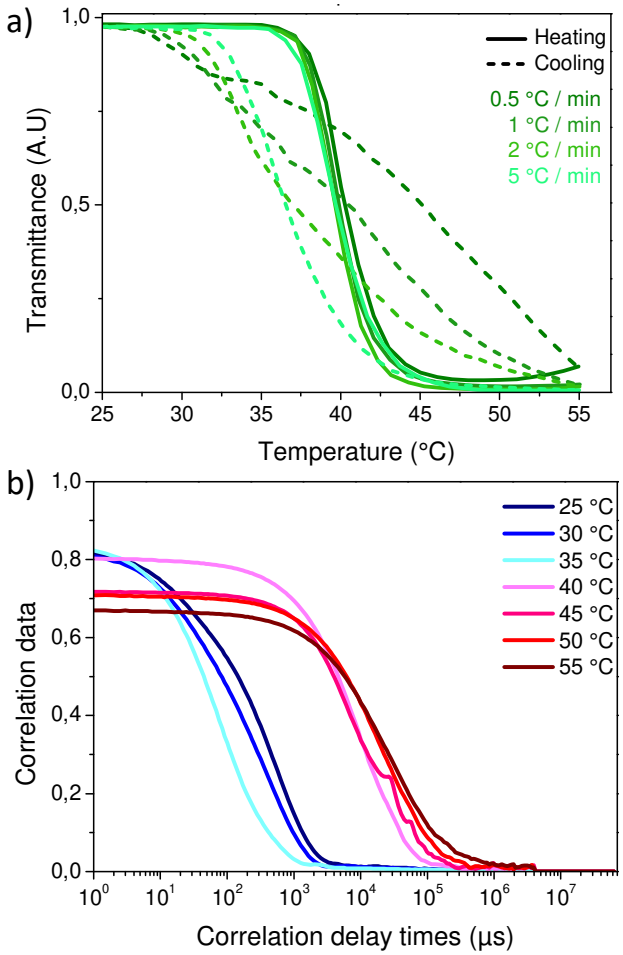

***Figure 4**. a) Turbidimetry and DLS measurements as a function of temperature of an aqueous solution of $PVAm_{10}$-b-$PNIPAM_{50}$@pH11 ($0.1\%_{w/v}$ and $1\%_{w/v}$ respectively). a) Transmittance monitored at 500 nm at different heating and cooling rates (0.5 - 1 - 2 - 5 °C/min), b) Evolution of correlation functions on heating between 25 °C and 55 °C.*

DLS analysis were then carried out to evidence the formation of aggregates and determine their sizes and stability. The correlation functions were plotted in **Figure 4b** at different temperatures. Above 35°C the shifting of the correlation curve towards longer correlation times clearly indicates the appearance of larger objects or aggregates. Both the loss in intensity observed above 45°C and the shape of the correlation curves suggest a poor colloidal stability of these objects and a sedimentation phenomenon (the precise determination of the morphology and size of aggregates will be further investigated in the next section). In order to have a further understanding of the mechanism behind this transition, ^{1}H NMR analysis was performed with a temperature increase from 20 °C to 55 °C (see **Figure 5**). First, a significant increase of chemical shift was measured as a function of temperature. Moreover, even if signals remained visible from 20 °C to 55 °C, the measured intensity dropped down along with temperature. Indeed, upon heating partial dehydration hampered chain mobility, inducing a shift of signals towards lower fields and a loss of the signal intensity [36-39]. The peaks did not completely disappear, probably due to the presence of residual water inside the aggregates.

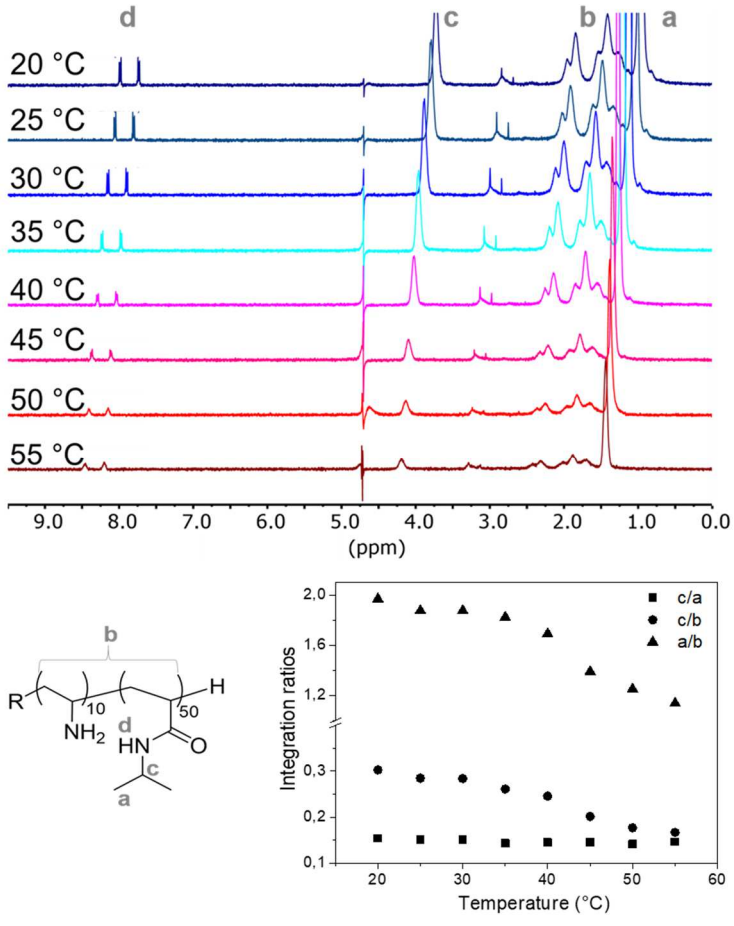

***Figure 5**. ^{1}H NMR spectra of $PVAm_{10}$-$PNIPAM_{50}$ block copolymer as a function of temperature (from 20 °C to 55 °C) and the corresponding evolution of ▲ a/b, ● c/b ratio and ■ c/a integration ratios block copolymer in D_2O at 1%$_{w/v}$).*

In order to highlight the influence of temperature on each block, the peak integrals corresponding to NIPAM monomer units (**a** and **c**) and backbone methylene protons of both blocks(**b**) were measured.

Figure 5b depicts the evolution of **c/a**, **c/b** and **a/b** integration ratios as a function of temperature. The ratio (**c/a**) corresponding to PNIPAM solely remains roughly constant whatever the temperature and the measured value of 0.16 is in good agreement with the theoretical value equal to 0.17. The evolution of the integration of the characteristics peaks of PNIPAM relatively to the one of the copolymer backbone was then studied by following **c/b** and **a/b** ratio. Initial ratio values at 20 °C were equal to 0.3 and 1.9 respectively and were in good agreement with theoretical ratios estimated from the composition of the block copolymer (0.28 and 1.7 respectively). Nevertheless, once T_c was reached a significant decrease of both ratios was measured. This suggests that PNIPAM blocks are present in more dehydrated regions of the aggregates than PVAm, which limits the relaxation phenomenon.

Thermoresponsiveness at pH near and lower than pKa (pH 8 and 5)

At pH 5, the $PVAm_m$ block is fully protonated (**Figure 3**). UV-Vis transmittance profiles at heating and cooling ramps of 0.5 °C/min are shown in **Figure S6**. $PVAm_{10}$-$PNIPAM_{50}$@*pH11* and $PVAm_{10}$-$PNIPAM_{50}$@*pH5* present very different cooling profiles. Whereas the transmittance of $PVAm_{10}$-$PNIPAM_{50}$@*pH11* falls from 100 % transmittance to 0 % with a sharp transition, $PVAm_{10}$-$PNIPAM_{50}$@*pH5* did not reach full opacity when heated at 0.5 °C/min. This could be ascribed to the formation at pH 5 of smaller aggregates which results in a decrease of scattered light intensity. In addition, the evolution of transmittance as a function of temperature, indicating a slower and more difficult solubilization of dehydrated PNIPAM in water at pH 11 than for lower pH. Lastly, the measured values of T_c at different pH tend, as expected, to decrease with an increase of pH. Above pKa at pH 11, the polyamine block is fully deprotonated and is indeed less hydrophilic than the its cationic version, resulting in a decrease of T_c from 42.2 °C at pH 5 to 39.8 °C (see Table S1). At an intermediate pH, $PVAm_{10}$-$PNIPAM_{50}$@*pH8* exhibited expected heating and cooling profiles with sharp slopes during both phases. DSC measurements revealed that the variation of enthalpy associated with the phase transition were -8.14 and -10.37 J per gram of PNIPAM at pH 5 and 8 respectively. At pH 11 it was reduced to -2.98 J/g suggesting a less energetically consuming dehydration which is consistent with a lower T_c value at pH 11 than pH 5. Consistently with turbidity measurements, scattering experiments showed notable differences between copolymer solutions at pH 5 and 11 (see **Figure 6** and Figure 4b respectively). Correlation functions of $PVAm_{10}$-$PNIPAM_{50}$@*pH5* are representative of objects with a larger polydispersity at 25 °C than at 45 °C (from 0.7 at 25 °C to 0.06 at 45 °C) suggesting a transition from an uncontrolled state of randomly formed objects to more organized objects. Interestingly above T_c, the estimated size of the aggregates formed at pH 5 from Z-av values (100 nm) are found to be significantly smaller than the ones estimated at pH 8 and 11 (in the µm range).

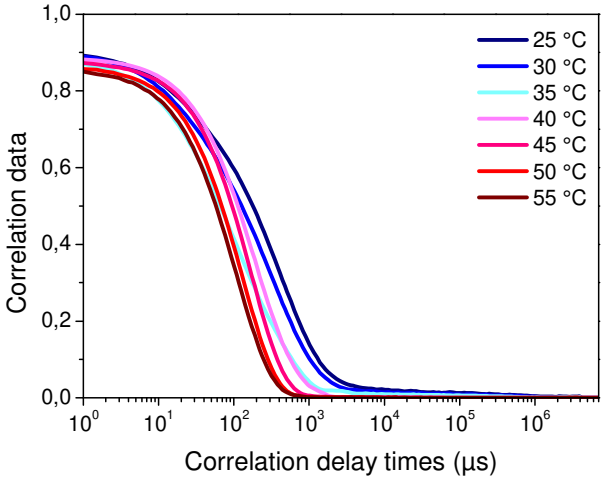

***Figure 6**. DLS measurements as a function of temperature of a 1%$_{w/v}$ aqueous solution of PVAm$_{10}$-b-PNIPAM$_{50}$@pH5 : evolution of correlation functions on heating between 25 °C and 55 °C.*

Comparative ^{1}H NMR studies as a function of temperature were further performed at pH < pKa, pH ~ pKa and pH > pKa and are presented in **Figure 7** at 25 °C and 45 °C (see also **Figure S7**). It is first noteworthy that the intensity of amide protons of PNIPAM at 8.0-8.3 ppm was higher at pH 11. This could be ascribed to a slower exchange phenomenon than at pH 5 and 8. Moreover, the observed trends as a function of temperature are very similar whatever the pH. At 20 °C, the measured **c/b** experimental ratio is close to the theoretical one (0.3 vs 0.28). With the increase of temperature, this ratio then gradually decreased to finally reach a value of 0.17 above T_c regardless of the pH value. This suggests that, whatever the pH, aggregates are formed with dehydrated PNIPAM blocks exhibiting more restricted motion than the PVAm ones.

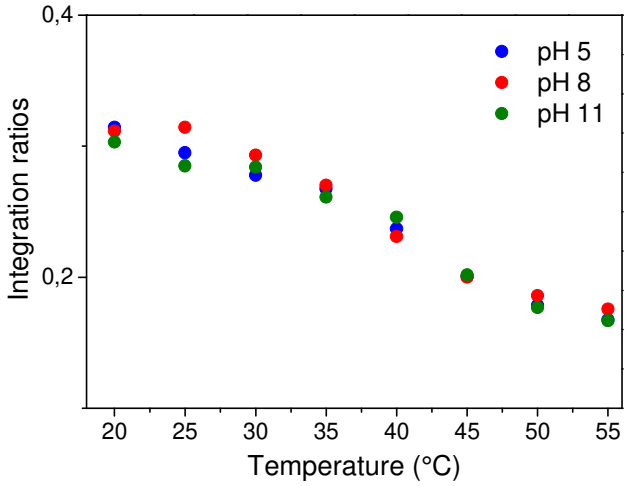

***Figure 7**. ^{1}H NMR of PVAm$_{10}$-PNIPAM$_{50}$ aqueous solutions: evolution of integration ratio **c/b** (as defined in Figure 5) as a function of temperature between 20 °C and 55°C at pH 5 (blue), pH 8 (red) and pH 11 (green).*

The zeta potential was then measured below and above T_c at different pH value (see **Table 2**). Under pKa at pH 5.6, the ξ-potential increased significantly between 25 °C and 45 °C from 8.9 to 27.4 mV. During the transition PNIPAM dehydrated and curled up on itself, exposing charged PVAm blocks to the outer surface of objects. The same transition occurred at pH above pKa but as the PVAm block was fully deprotonated no change in ξ-potential was noticeable between 25 and 45°C (-7.4 and -11.9 mV respectively).

Influence of the molar mass of PVAm-b-PNIPAM copolymer on thermoresponsive properties

To evaluate the influence of chain length on physicochemical properties, all previous characterizations were also performed on the $PVAm_{20}$-*b*-$PNIPAM_{100}$ block copolymer. It should be noted that copolymers in this study are homothetic in their composition. T_c values obtained from different characterization techniques were gathered in **Table 2** (see also **Table S1**). It appeared that T_c was not significantly affected by the copolymer chain length. At pH 11, scattering experiments evidenced the formation of large objects that have a tendency to precipitate as already observed for $PVAm_{10}$-*b*-$PNIPAM_{50}$. Nevertheless, from turbidimetry measurements comparatively to $PVAm_{10}$-*b*-$PNIPAM_{50}$, a sharper cooling transition is observed for $PVAm_{20}$-*b*-$PNIPAM_{100}$ copolymer (**Figure S8**). ^{1}H NMR studies as a function of temperature did not show noticeable differences for polymers of different chain lengths (see Figure 5 and Figure 8 for comparison). At pH 6, turbidimetry and scattering experiments (**Figure S8**) also demonstrated the formation of large colloids above T_c but with a smaller size than at pH 11. Consequently, the scattered light remained low above T_c and transmittance remained above 0. ξ-potential measurements of $PVAm_{20}$-*b*-$PNIPAM_{100}$ showed the same trend as a function of temperature and pH than for the shorter $PVAm_{10}$-$PNIPAM_{50}$. To conclude, apart from kinetic considerations on the hydration/dehydration mechanism, the block copolymer chain length did not significantly affect T_c values and the structure of the observed colloids.

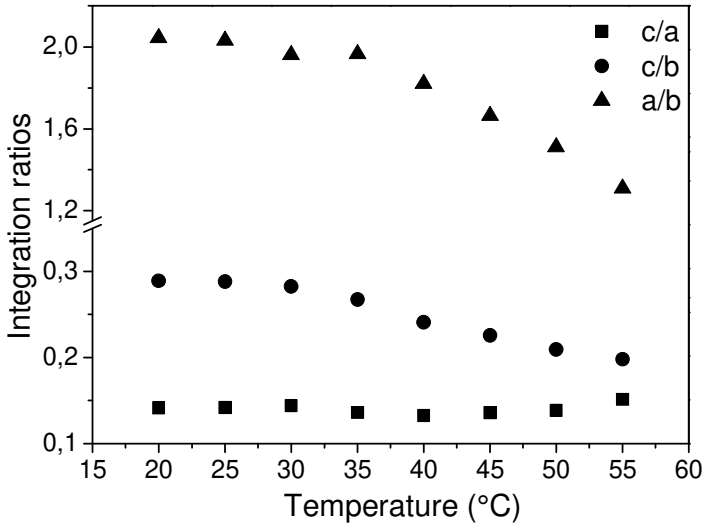

Figure 8. *^{1}H NMR spectra of $PVAm_{20}$-$PNIPAM_{100}$ block copolymer as a function of temperature (from 20 °C to 55 °C): evolution of ▲ a/b, ● c/b and ■ c/a integration ratios (a,b and c are defined in Figure 5), block copolymer in D_2O at 1%$_{w/v}$).*

Table 2*. Main physicochemical properties of $PVAm_m$-b-$PNIPAM_n$ copolymers: T_c values determined from (a) turbidimetry measurements during heating ramp and extrapolated at 0 °C/min, (b) Z-av onset point in DLS heating ramp, (c) Derived Count Rate (DCR) onset point in DLS heating ramp and (d) DSC during heating ramp and extrapolated at 0 °C/min; (e) enthalpy variation per gram of PNIPAM obtained from DSC at different heating rates and extrapolated to 0°C/min; zeta-potential values (associated standard deviations are given in supporting information)*

				$PVAm_m$-*b*-$PNIPAM_n$ properties			
	pH	*T_c (°C) UV-Vis[a]*	*T_c (°C) DLS, Z-av[b]*	*T_c (°C) DLS, DCR[c]*	*T_c (°C) DSC[d]*	*ΔH (J/g per units[e]*	*ζ-potential (mV)[f] 25°C/45°C*
$PVAm_{10}$-*b*-$PNIPAM_{50}$	5	42 ±1	37.0±0.5	37.5±0.5	38.6±0.2	-8	8.9/27.4
	11	40±1	37.5±0.5	36.0±0.5	37.5±0.2	-3	-7.4/-11.9
$PVAm_{20}$-*b*-$PNIPAM_{100}$	5	39±1	34.7±0.5	42.0±0.5	37.3±0.2	-8	18.4/34.6
	11	40±1	35.0±0.5	37.3±0.5	36.9±0.2	-3	-4.1/-2.1

Conclusion on thermoresponsive properties.

T_c values obtained from the different methods were reported in Table 2b and were generally higher at pH 5 than pH 11 as expected considering the stronger hydrophilicity of protonated PVAm compared to the deprotonated version. T_c values were not remarkably influenced by the molar mass of polymers and neither were ζ-potentials. Whatever the pH, PVAm-*b*-PNIPAM copolymers remain thermoresponsive. Nevertheless, pH strongly influenced the kinetics of aggregation/disassembly and it seems that at low pH, smaller and more defined aggregates are prone to be formed. ^{1}H NMR analysis also evidenced the modification of polymer motion induced by the change of temperature that might result in the formation of large objects with PNIPAM blocks located in regions with restricted motion capability. In the following section, based on these first results, we will investigate the formation of colloidal structures induced by the change of temperature through TEM, multiangle DLS and SAXS experiments.

3.3 Colloid characterization

The study of the cloud point transition had already highlighted significant differences in the behaviour of $PVAm_{10}$-*b*-$PNIPAM_{50}$ at pH 5 and 11. More precisely it appears that more defined and smaller nano-objects tend to be formed at pH lower than pKa (**Figure S9** of ESI). To confirm this, multi-angle DLS, TEM and SAXS experiments were carried out at pH 5 and 11.

At pH 11, the evolution of hydrodynamic diameter as a function of temperature was first analysed by multi-angle DLS (**Figure 9**a). Below T_c, a hydrodynamic diameter equal to 116 ± 60 nm is evaluated. Above T_c, D_h reached a maximum value of 361 nm at 40 °C and then decreased to 150 ± 10 nm at 55 °C. TEM analysis performed on samples deposited at 25°C showed entangled elongated non-spherical structures (**Figure S10a**) whose partial aggregation might result on the aggregates observed with DLS. At 45 °C, TEM images showed large well-defined spherical objects of 58 ± 10 nm (**Figure 9**b and corresponding size distribution in **Figure S10**). At this temperature, the absence of very large aggregates in dried samples might suggest that the observed colloids through scattering experiments might result from the aggregation of smaller colloids without reorganization of polymer chains between them. This mechanism is similar to the one observed for other families of block copolymers involving the formation of mesoglobules [20,35] and enables the fast disruption of aggregates below T_c. The formation of mesoglobules might be promoted here by the dehydration induced by the increase of temperature. Interestingly as can be seen in **Figure 9**a, depending on the targeted temperature, different hydrodynamic diameters were measured above T_c: the higher the temperature, the smaller the mesoglobules.

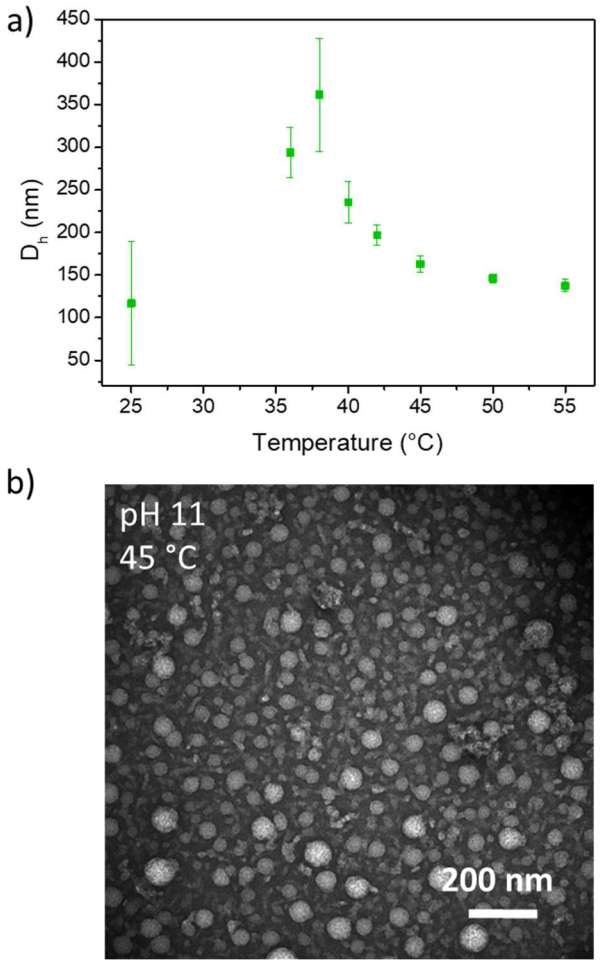

Figure 9. *a) Multi-angle DLS analysis: evolution of the estimated hydrodynamic diameter as a function of temperature from 25 to 55 °C of a $PVAm_{10}$-b-$PNIPAM_{50}$@pH11 aqueous solution at 0.01%$_{w/v}$.Measurements were carried at each temperature with a return to ambient temperature in between. b) TEM image of $PVAm_{10}$-b-$PNIPAM_{50}$@pH11 deposited on a copper-carbon grid from a solution at 0.1%$_{w/v}$ at 45 °C*

SAXS measurements were performed on $PVAm_{10}$-*b*-$PNIPAM_{50}$ at 1 %$_{w/v}$ as a function of temperature (**Figure 10**). Scattering curves showed an increase of I(q) from 20 °C to 35 °C followed by a decrease at higher temperatures. In the middle q region, I(q) followed a power law with $I(q) \sim q^{-\alpha}$ with a coefficient α of 2.13 at 25 °C and 3.03 at 45 °C, suggesting a densification of aggregates. This observation is in accordance with DLS results which showed the aggregation of preexisting smaller aggregates above T_c. Moreover, SAXS confirmed the uncontrolled behaviour of this aggregation phenomenon as no defined morphologies could be identified. Therefore, at pH 11, block copolymers exist as aggregates generated by the interaction between PNIPAM and PVAm block. Increasing the temperature above T_c induced the formation of larger, denser and poorly defined aggregates.

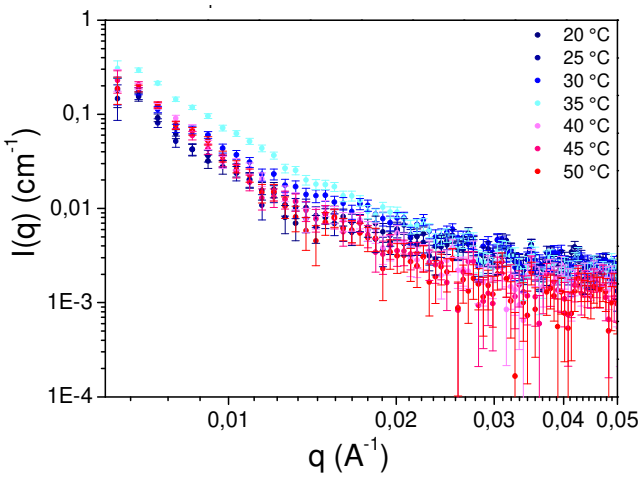

***Figure 10**. Scattering curves of $PVAm_{10}$-$PNIPAM_{50}$ at pH 11 as a function of temperature from 20 °C to 50 °C*

At pH 5, the PVAm block is fully protonated. Average D_h values measured by multi-angle DLS as a function of temperature are plotted in **Figure 11**. $PVAm_{10}$-*b*-$PNIPAM_{50}$ spontaneously assembled at 25 °C into polydisperse objects with a 150 nm average diameter. In a dried state, spherical particles with a mean diameter of 19 ± 2 nm were observed by TEM (**Figure 12**, left). Mori *et al.* reported that room temperature self-assembly could be induced by PVAm ability to form inter- and intra-hydrogen bonds [31]. This suggests that at 25°C large and poorly defined colloids measured by DLS could be obtained from the aggregation through hydrogen bonding of smaller block copolymer aggregates. Interestingly, at higher temperature smaller colloids were observed with an average hydrodynamic diameter D_h = 70 ± 5 nm (at 55°C). Consistently with correlation functions showed in **Figure 6**, polydispersity decreased with an increase of temperature, suggesting a more organized state above T_c, and a random one below T_c. In TEM, at 45 °C, spherical particles were visualized with a mean diameter of 24 ± 3 nm (**Figure 12**, right). As discussed in the previous section, the formation of better defined nano-objects at higher temperature might result from the aggregation of amphiphilic $PVAm_{10}$-*b*-$PNIPAM_{50}$, PNIPAM being hydrophobic above T_c. The presence at the surface of these colloids of positively charged PVA_m blocks evidenced by positive zeta-potential measurements can prevent their further aggregation.

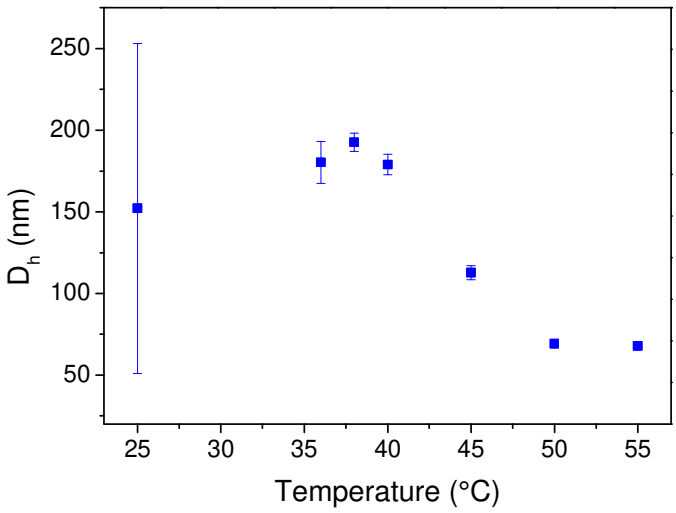

***Figure 11**. Multi-angle DLS measurements: evolution of estimated hydrodynamic diameter as a function of temperature from 25 °C to 55 °C of a $PVAm_{10}$-b-$PNIPAM_{50}$ aqueous solution ($1\%_{w/v}$) at pH 5. Measurements were carried out at each temperature with a return to ambient temperature in between.*

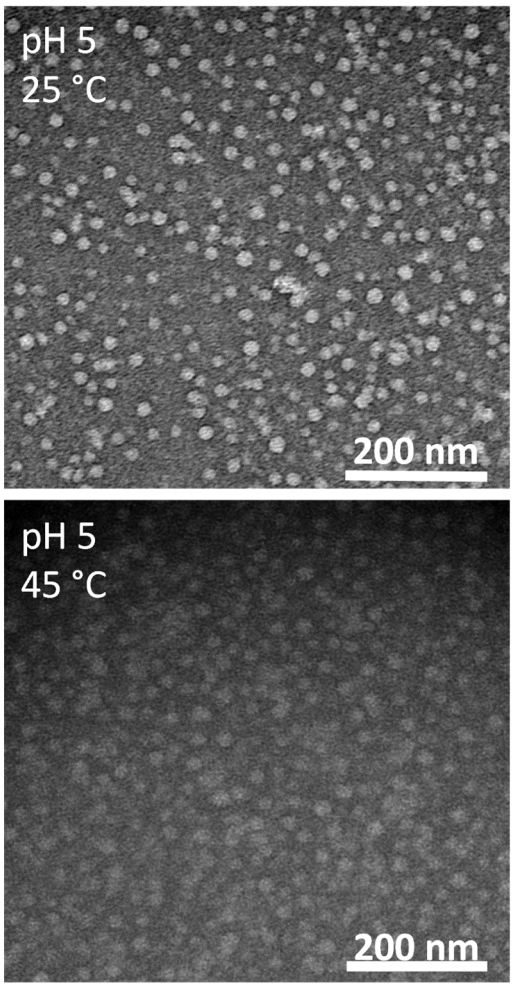

***Figure 12**. TEM image of $PVAm_{10}$-b-$PNIPAM_{50}$ at pH 5 deposited on a copper-carbon grid from a solution at $0.1\%_{w/v}$ at 25 and 45 °C*

SAXS measurement was carried out to further investigate the morphology of aggregates. Scattering curve profiles as a function of temperature (**Figure 13a**) indicated a transition from fractal-like

aggregates at T <T_c to nano-objects above T_c, with still some residual aggregates as I(q) did not stabilize in the small q region. The comparison of SAXS profiles at pH 5 and 11 at 25 °C and 45 °C (**Figure 13b**) clearly showed the difference of behaviour as a function of the protonation degree of the PVAm block. In the middle q region, at pH 5 signals of the $PVAm_{10}$-*b*-$PNIPAM_{50}$ copolymer followed the power law $I(q) \sim q^{-\alpha}$, with α decreasing from 2.4 at 25 °C to 1.72 at 45 °C. Assuming a dense core/hydrated shell model an average diameter of 30 nm was obtained for the inner core of PNIPAM suggesting a thickness for PVAM shell equal to 20 nm (i.e. an overall diameter of 70 nm). Assuming a density for the dense PNIPAM core equal to 1.1 g/cm^3 (ρ_{PNIPAM}) and knowing the average molar mass of PNIPAM (M_{PNIPAM}) and Avogadro constant (N_A) an aggregation number equal to 1600 was calculated using the following equation: $N_{agg} = \frac{4\pi.\rho_{PNIPAM}.R^3_{PNIPAM}.N_A}{3M_{PNIPAM}}$. [17]

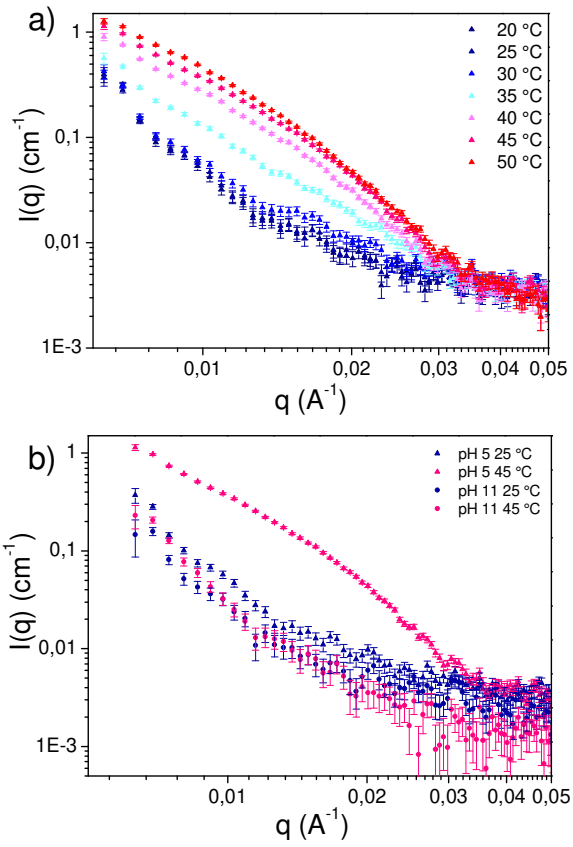

***Figure 13**. Scattering curves of a) $PVAm_{10}$-b-$PNIPAM_{50}$ at pH 5 as a function of temperature from 20 °C to 50 °C and of b) $PVAm_{10}$-b-$PNIPAM_{50}$ at pH5 (▲) and pH11 (●) at 25 °C (blue) and 45 °c (pink).*

In conclusion at pH 5, whereas poorly defined aggregates were observed for T < T_c, an increase of temperature above T_c led to the formation of better defined nano-objects. At high temperature, scattering experiments along with NMR results and zeta potential measurements suggest the formation of colloids comprising a PNIPAM dehydrated core with an outer charged shell issued from

protonated PVAm with an average aggregation number of 1600 polymer chains per nano-object. Finally, the SAXS study was also performed on $PVAm_{20}$-$PNIPAM_{100}$ and revealed a very similar behaviour with aggregates at pH 11 and the transition from aggregates to self-assembled nano-objects at pH 5 over the critical transition (**Figure S11**). On the basis of the obtained results at pH 5 and pH 11, a schematic phase diagram of the aggregates morphologies of $PVAm_{10}$-*b*-$PNIPAM_{50}$ as a function of pH and temperature can be proposed as depicted in **Figure 14**.

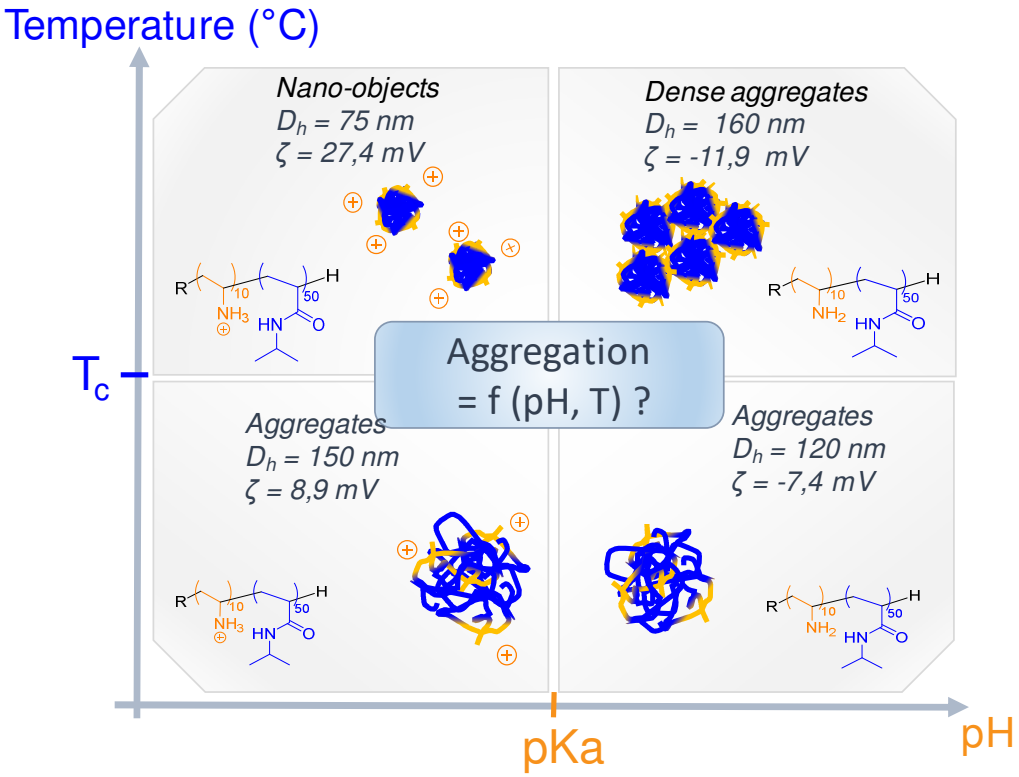

Figure 14 Schematic representation of the proposed phase diagram based on scattering measurements and TEM images of $PVAm_{10}$-b-$PNIPAM_{50}$ at pH </ > pKa and T </> T_c

4. Conclusion

$PVAm_m$-*b*-$PNIPAM_n$ copolymers were synthesized by hydrazinolysis of $PVPI_m$-*b*-$PNIPAM_n$ precursors obtained by RAFT polymerization. The experimental compositions and molar masses of the obtained diblock copolymers were very close to $PVAm_{10}$-*b*-$PNIPAM_{50}$ and $PVAm_{20}$-*b*-$PNIPAM_{100}$ targeted structures. This family of copolymers has a double-hydrophilic character and is both pH- and thermoresponsive. This double feature brings them interesting aggregation properties which we studied in this work with a thorough physico-chemical characterization. First, the transition in temperature was studied by the determination of T_c at different pHs (i.e pH < pKa and pH > pKa) and different methods (turbidimetry, DLS, DSC). As expected, we showed that T_c is higher at low pH as the protonated PVAm block is more hydrophilic than its neutral analog. The comparison of $PVAm_{10}$-*b*-$PNIPAM_{50}$ and $PVAm_{20}$-*b*-$PNIPAM_{100}$ did not reveal major differences, a result that can be explained since PNIPAM is a type-II LCST polymer whose T_c is not affected by molar mass. Light and X-ray scattering experiments, along with TEM, confirmed this spontaneous aggregation at $T < T_c$ and revealed polydisperse fractal-like aggregates with D_h of 150 nm at pH < pKa and 120 nm at pH > pKa. Above T_c, the aggregation of copolymers is mostly influenced by the protonation state of the PVAm block. In its protonated form i.e. below pKa, core-shell particles were revealed with a dense PNIPAM core and a hydrophilic cationically charged and repulsive shell which prevented further aggregation and resulted in a monodisperse population. Above the pKa of PVAm, an aggregation of pre-existing aggregates, was observed. This study confirmed the pH- and thermoresponsive properties of PVAm-*b*-PNIPAM diblock copolymers which make them great candidates for surface modification applications.

Aknowledgements

The authors would like to thank Barbara Lonetti and Christophe Mingotaud for their help in the discussion of SAXS and DLS results respectively.

References

[1] J.K. Kim, S.Y. Yang, Y. Lee, Y. Kim, Functional nanomaterials based on block copolymer self-assembly, Prog. Polym. Sci. 35 (2010) 1325–1349. https://doi.org/10.1016/j.progpolymsci.2010.06.002.

[2] Z. Xu, L. Wang, F. Fang, Y.F. and Z. Yin, A Review on Colloidal Self-Assembly and their Applications, Curr. Nanosci. (2016).

[3] P. Samaddar, A. Deep, K.-H. Kim, An engineering insight into block copolymer self-assembly: Contemporary application from biomedical research to nanotechnology, Chem. Eng. J. 342 (2018) 71–89. https://doi.org/10.1016/j.cej.2018.01.062.

[4] M. Khimani, H. Patel, V. Patel, P. Parekh, R.L. Vekariya, Self-assembly of stimuli-responsive block copolymers in aqueous solutions: an overview, Polym. Bull. (2019). https://doi.org/10.1007/s00289-019-03046-w.

[5] M. Wei, Y. Gao, X. Li, M.J. Serpe, Stimuli-responsive polymers and their applications, Polym. Chem. 8 (2016) 127–143. https://doi.org/10.1039/C6PY01585A.

[6] F. Doberenz, K. Zeng, C. Willems, K. Zhang, T. Groth, Thermoresponsive polymers and their biomedical application in tissue engineering – a review, J. Mater. Chem. B. 8 (2020) 607–628. https://doi.org/10.1039/C9TB02052G.

[7] M.A. Ward, T.K. Georgiou, Thermoresponsive Polymers for Biomedical Applications, Polymers. 3 (2011) 1215–1242. https://doi.org/10.3390/polym3031215.

[8] N.A. Cortez-Lemus, A. Licea-Claverie, Poly(N-vinylcaprolactam), a comprehensive review on a thermoresponsive polymer becoming popular, Prog. Polym. Sci. 53 (2016) 1–51. https://doi.org/10.1016/j.progpolymsci.2015.08.001.

[9] N. Badi, Non-linear PEG-based thermoresponsive polymer systems, Prog. Polym. Sci. 66 (2017) 54–79. https://doi.org/10.1016/j.progpolymsci.2016.12.006.

[10] A.P. Constantinou, T.K. Georgiou, Thermoresponsive gels based on ABC triblock copolymers: effect of the length of the PEG side group, Polym. Chem. 7 (2016) 2045–2056. https://doi.org/10.1039/C5PY02072G.

[11] W. Steinhauer, R. Hoogenboom, H. Keul, M. Moeller, Block and Gradient Copolymers of 2-Hydroxyethyl Acrylate and 2-Methoxyethyl Acrylate via RAFT: Polymerization Kinetics, Thermoresponsive Properties, and Micellization, Macromolecules. 46 (2013) 1447–1460. https://doi.org/10.1021/ma302606x.

[12] X. Xiang, X. Ding, N. Chen, B. Zhang, P.A. Heiden, End group polarity and block symmetry effects on cloud point and hydrodynamic diameter of thermoresponsive block copolymers, J. Polym. Sci. Part Polym. Chem. 53 (2015) 2838–2848. https://doi.org/10.1002/pola.27757.

[13] A. Laschewsky, E.D. Rekaï, E. Wischerhoff, Tailoring of Stimuli-Responsive Water Soluble Acrylamide and Methacrylamide Polymers, Macromol. Chem. Phys. 202 (2001) 276–286. https://doi.org/10.1002/1521-3935(20010101)202:2<276::AID-MACP276>3.0.CO;2-1.

[14] A. Halperin, M. Kröger, F.M. Winnik, Poly(N-isopropylacrylamide) Phase Diagrams: Fifty Years of Research, Angew. Chem. Int. Ed. 54 (2015) 15342–15367. https://doi.org/10.1002/anie.201506663.

[15] S. Chen, K. Wang, W. Zhang, A new thermoresponsive polymer of poly(N-acryloylsarcosine methyl ester) with a tunable LCST, Polym. Chem. 8 (2017) 3090–3101. https://doi.org/10.1039/C7PY00274B.

[16] M. Heskins, J.E. Guillet, Solution Properties of Poly(N-isopropylacrylamide), J. Macromol. Sci. Part - Chem. 2 (1968) 1441–1455. https://doi.org/10.1080/10601326808051910.

[17] S. Sistach, M. Beija, V. Rahal, A. Brûlet, J.-D. Marty, M. Destarac, C. Mingotaud, Thermoresponsive Amphiphilic Diblock Copolymers Synthesized by MADIX/RAFT: Properties in Aqueous Solutions and Use for the Preparation and Stabilization of Gold Nanoparticles, Chem. Mater. 22 (2010) 3712–3724. https://doi.org/10.1021/cm100674p.

[18] Z.-P. Xiao, Z.-H. Cai, H. Liang, J. Lu, Amphiphilic block copolymers with aldehyde and ferrocene-functionalized hydrophobic block and their redox-responsive micelles, J. Mater. Chem. 20 (2010) 8375–8381. https://doi.org/10.1039/C0JM01453B.

[19] A. S. Hoffman, P. S. Stayton, V. Bulmus, G. H. Chen, J. P. Chen, C. Cheung, A. Chilkoti, Z. L. Ding, L. C. Dong, R. Fong, C. A. Lackey, C. J. Long, M. Miura, J. E. Morris, N. Murthy, Y. Nabeshima, T. G. Park, O. W. Press, T. Shimoboji, S. Shoemaker, H. J. Yang, N. Monji, R. C. Nowinski, C. A. Cole, J. H. Priest, J. M. Harris, K. Nakamae,T. Nishino,T. Miyata, Really smart bioconjugates of smart polymers and receptor proteins, J. Biomed. Mater. Res. 52 (2000) 577-586. https://doi.org/10.1002/1097-4636(20001215)52:4%3C577::AID-JBM1%3E3.0.CO;2-5

[20] E. Read, B. Lonetti, S. Gineste, A.T. Sutton, E. Di Cola, P. Castignolles, M. Gaborieau, A.-F. Mingotaud, M. Destarac, J.-D. Marty, Mechanistic insights into the formation of polyion complex aggregates from cationic thermoresponsive diblock copolymers, J. Colloid Interface Sci. 590 (2021) 268–276. https://doi.org/10.1016/j.jcis.2021.01.028.

[21] G.-F. Luo, W.-H. Chen, X.-Z. Zhang, 100th Anniversary of Macromolecular Science Viewpoint: Poly(N-isopropylacrylamide)-Based Thermally Responsive Micelles, ACS Macro Lett. 9 (2020) 872–881. https://doi.org/10.1021/acsmacrolett.0c00342

[22] M. D. C. Topp, P. J. Dijkstra, H. Talsma, J. Feijen, Thermosensitive Micelle-Forming Block Copolymers of Poly(ethylene glycol) and Poly(N-isopropylacrylamide), Macromolecules, 30 (1997), 8518–8520. https://doi.org/10.1021/ma9710803.

[23] W. Zhang, L. Shi, K. Wu, Y. An, Thermoresponsive Micellization of Poly(ethylene glycol)-b-poly(N-isopropylacrylamide) in Water, Macromolecules 38 (2005), 5743–5747. https://doi.org/10.1021/ma0509199.

[24] J. Chen, B. Yan, X. Wang, Q. Huang, T. Thundat, H. Zeng, Core cross-linked double hydrophilic block copolymer micelles based on multiple hydrogen-bonding interactions, Polym. Chem., 8 (2017) 3066-3073. https://doi.org/10.1039/C7PY00210F

[25] K. Hales, D.J. Pochan, Using polyelectrolyte block copolymers to tune nanostructure assembly, Curr. Opin. Colloid Interface Sci. 11 (2006) 330–336. https://doi.org/10.1016/j.cocis.2006.12.004.

[26] A.P. Constantinou, T.K. Georgiou, Thermoresponsive Multiblock Copolymers: Chemistry, Properties and Applications, in: Temp.-Responsive Polym., John Wiley & Sons, Ltd, 2018: pp. 35–65. https://doi.org/10.1002/9781119157830.ch2.

[27] R. Pelton, Polyvinylamine: A Tool for Engineering Interfaces, Langmuir. 30 (2014) 15373–15382. https://doi.org/10.1021/la5017214.

[28] Y. Maki, H. Mori, T. Endo, Controlled RAFT Polymerization of N-Vinylphthalimide and its Hydrazinolysis to Poly(vinyl amine), Macromol. Chem. Phys. 208 (2007) 2589–2599. https://doi.org/10.1002/macp.200700330.

[29] Y. Maki, H. Mori, T. Endo, Controlled Synthesis of Alternating Copolymers by RAFT Copolymerization of N-Vinylphthalimide with N-Isopropylacrylamide, Macromol. Chem. Phys. 211 (2010) 1137–1147. https://doi.org/10.1002/macp.200900544.

[30] Y. Maki, H. Mori, T. Endo, Synthesis of Amphiphilic and Double-Hydrophilic Block Copolymers Containing Poly(vinyl amine) Segments by RAFT Polymerization of N-Vinylphthalimide, Macromol. Chem. Phys. 211 (2010) 45–56. https://doi.org/10.1002/macp.200900332.

[31] R. Kanto, R. Yonenuma, M. Yamamoto, H. Furusawa, S. Yano, M. Haruki, H. Mori, Mixed Polyplex Micelles with Thermoresponsive and Lysine-Based Zwitterionic Shells Derived from Two Poly(vinyl amine)-Based Block Copolymers, Langmuir. 37 (2021) 3001–3014. https://doi.org/10.1021/acs.langmuir.0c02197.

[32] X. Liu, O. Coutelier, S. Harrisson, T. Tassaing, J.-D. Marty, M. Destarac, Enhanced Solubility of Polyvinyl Esters in scCO2 by Means of Vinyl Trifluorobutyrate Monomer, ACS Macro Lett. 4 (2015) 89–93. https://doi.org/10.1021/mz500731p.

[33] A. Glaria, M. Beija, R. Bordes, M. Destarac, J.-D. Marty, Understanding the Role of ω-End Groups and Molecular Weight in the Interaction of PNIPAM with Gold Surfaces, Chem. Mater. 25 (2013) 1868–1876. https://doi.org/10.1021/cm400480p.

[34] S. Kobayashi, K.D. Suh, Y. Shirokura, Chelating ability of poly(vinylamine): effects of polyamine structure on chelation, Macromolecules. 22 (1989) 2363–2366. https://doi.org/10.1021/ma00195a062.

[35] F. Yin, J.S. Behra, M. Beija, A. Brûlet, J. Fitremann, B. Payré, S. Gineste, M. Destarac, N. Lauth-de Viguerie, J.-D. Marty, Effect of the microstructure of n-butyl acrylate/N-isopropylacrylamide copolymers on their thermo-responsiveness, self-organization and gel properties in water, J. Colloid Interface Sci. 578 (2020) 685–697. https://doi.org/10.1016/j.jcis.2020.06.005.

[36] F. Yin, H. H. Nguyen, O. Coutelier, M. Destarac, N. Lauth-de Viguerie, J.-D. Marty, Effect of copolymer composition of controlled (N-vinylcaprolactam/N-vinylpyrrolidone) statistical copolymers on formation, stabilization, thermoresponsiveness and catalytic properties of gold nanoparticles, Colloids and Surfaces A: Physicochemical and Engineering Aspects, 630 (2021) 127611. https://doi.org/10.1016/j.colsurfa.2021.

[37] T. Tokuhiro, T. Amiya, A. Mamada, T. Tanaka, NMR study of poly(N-isopropylacrylamide) gels near phase transition, Macromolecules. 24 (1991) 2936–2943. https://doi.org/10.1021/ma00010a046.

[38] C.M. Burba, S.M. Carter, K.J. Meyer, C.V. Rice, Salt Effects on Poly(N-isopropylacrylamide) Phase Transition Thermodynamics from NMR Spectroscopy, J. Phys. Chem. B. 112 (2008) 10399–10404. https://doi.org/10.1021/jp8005553.

[39] J. Spěváček, Application of NMR Spectroscopy to Study Thermoresponsive Polymers, in: Temp.-Responsive Polym., John Wiley & Sons, Ltd, 2018: pp. 225–247. https://doi.org/10.1002/9781119157830.ch9.